sp- and *d*-band effects on secondary low-energy electron generation

V. Desbuis,[1] D. Lacour,[1] C. Tiusan,[2] W. Weber,[3] and M. Hehn[1,*]
[1]*Institut Jean Lamour, CNRS, Université de Lorraine, F-54000 Nancy, France*
[2]*Department of Solid State Physics and Advanced Technologies, Faculty of Physics, Babes-Bolyai University, Cluj Napoca 400114, Romania*
[3]*Institut de Physique et Chimie des Matériaux de Strasbourg, UMR 7504 CNRS, Université de Strasbourg, 23 Rue du Loess, Boîte Postale 43, 67034 Strasbourg Cedex 2, France*

(Received 20 June 2023; revised 22 September 2023; accepted 14 November 2023; published 20 December 2023)

Ballistic hot electrons are extracted from a magnetic tunnel junction and injected into a metallic base with energies ranging from 0.65 to 2.8 eV. The energy and wave vector analysis made by a low height Si/Cu Schottky barrier allows one to disentangle the different contributions to the scattering. The hot electrons transport is interpreted as being mainly influenced by inelastic scattering. An explicit transport model reproduces our measurements and explains them as resulting directly from an electron-electron inelastic scattering process related to the *sp* and *d* bands of the ferromagnetic material involved.

DOI: 10.1103/PhysRevB.108.214424

I. INTRODUCTION

Hot electrons are charge carriers excited above the Fermi level. Studied for more than 50 years in semiconductors, from Gunn diodes to integrated circuit diagnostics [1–5], hot electrons play an important role in many other fields such as high efficiency photovoltaics [6], photoinduced surface reactions [7], spin transfer torque [8] or ultrafast demagnetization [9] in nanomagnetism, among others. Our understanding of their properties thus opens the way to multidisciplinary applications, such as energy conversion, photocatalysis, photodetection, quantum chemistry, or optically active materials. Among the parameters that dictate their transport properties in materials, the electronic band structure is one of the most important because it defines the transitions between energy levels and thus the interactions between electrons.

Probing the electronic energy states by photoexcitation is a common method. Photoemission and associated derived techniques [10–14] have been used to verify theoretical expectations [15]. However, to be extracted from a solid, the electron must have an energy greater than the work function of the material. Hence, low-energy measurements cannot be performed using the aforementioned methods. Two-photon photoemission addresses some of these limitations by providing access to the lifetimes of hot electrons [16] but not to their transport properties. A further step is taken by using ballistic electron energy microscopy (BEEM) [17,18] or so-called "all-solid-state" devices such as the spin valve transistor (SVT) [19,20] or the magnetic tunnel transistor (MTT) [21,22]. These last techniques rely on the same idea: only electrons with high enough energy and a momentum perpendicular to the interfaces can access available states of semiconductor composing a Schottky diode. BEEM experiments, using a scanning tunneling microscopy tip for electron injection, have proven to be an effective method for measuring the mean free path in several materials [23,24]. Furthermore, experimental results [25,26] supported by extensive theoretical work based on the band structure of materials [27] have demonstrated the ballistic behavior of electrons collected in these multilayer systems. Most BEEM results have been interpreted by considering inelastic scattering of hot electrons as the main source of features in the ballistic current spectra [28] and only [29] mentions the contribution of secondary electrons to the collected current. When probing transition metals such as Fe, Co, or Ni, an effect induced by the *d* band is to be expected since the increase of the electron density associated with this band takes place at about 1 eV below the Fermi level; i.e., in an accessible energy range. However, such an influence of the band has not yet been demonstrated in transport experiments based on BEEM, SVT, or MTT.

In this paper, we present an analysis based on the contribution of secondary electrons to the current collected in a MTT. We interpret our experimental data set by considering both electron-electron interactions and an idealized band structure. An explicit transport model shows that our measurements result from a direct implication of a *d*-band scattering process in the CoFeB and [Co/Ni] layers.

II. ALL-SOLID-STATE DEVICE

In order to analyze the low-energy transport regime, we used an MTT architecture [30–32]. Our lab-on-a-chip hosts a magnetic tunnel junction which allows us to control and vary the injection energy of the electrons, a spin valve base, and a Schottky diode (Fig. 1). Changing the bias voltage across the tunnel barrier fixes the injection energy of charge carriers into the spin valve. The injected electrons are called primary electrons. The Schottky diode allows a double analysis: Firstly, by selecting in energy the electrons collected in

*Corresponding author: michel.hehn@univ-lorraine.fr

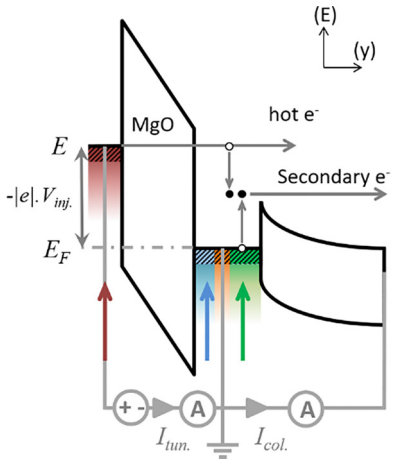

FIG. 1. All-solid-state device based on a magnetic tunnel transistor. See text for further details.

the semiconductor: only those with an energy higher than 0.7 eV are collected; secondly, in wave vector, thanks to an acceptance cone of less than 10° [33], defined with respect to the normal of the interface plane. The typical stack used in this study is as follows: Pt(5)/IrMn (7.5)/Co(2)/Ta(0.5)/CoFeB(2)/MgO(2.5)/CoFeB(y)/Cu(3.5)/[Ni(0.6)/Co(0.2)]x5/Ni(0.6)/Cu(5)/Ta(1)/Cu(5)//Si[100], where the numbers in brackets indicate the layer thicknesses in nanometers. Two values of y have been used: 1 and 4 nm. This device has been designed to address a much wider scope of effects related to spin-dependent transport including hot electrons spin precession [30–32], which requires such a complex structure. Here, we have restricted this study to the saturated state in order to simplify the analysis of the results. In this case, as all magnetizations are saturated and parallel, an electron flow consisting of mainly majority spins is considered with values of the electrons mean free path and/or attenuation length equal to that of majority-spin electrons in the considered materials.

III. MODEL FOR ELECTRON TRANSPORT

In order to model the electronic transport through our MTT (from left to right in Fig. 1), we distinguish three main steps as done in [25,34]. In a first step, hot electrons, also called primary electrons, are extracted from the tunnel barrier into the base. This generates a peaky electronic distribution at around $|e|\,V_{\text{inj}} - E_F$ at the base entrance (e is the elementary charge and V_{inj} the voltage applied to the tunnel barrier). The injected electron beam will be considered monokinetic with wave vector $\boldsymbol{k}$ perpendicular to the interfaces. The measured tunneling current, $I_{\text{tun}}(V_{\text{inj}})$, will be used to evaluate the transfer ratio $\text{TR} = \frac{I_{\text{col}}}{I_{\text{tun}}}$ where $I_{\text{col}}(V_{\text{inj}})$ is the current measured in the Si collector.

In a second step, the charge carriers transported through the base will be described within a free-electron approximation. As the metallic layer thicknesses are smaller or of the same order of magnitude as attenuation lengths, scattering should be accurately described using an exponential decay of the ballistic electron population all along the base. Matthiessen's rule provides an expression for the electrons mean free paths considering the different scattering processes involved:

$$\frac{1}{\lambda} = \frac{1}{\lambda_e(E)} + \frac{1}{\lambda_{\text{ph}}(T)} + \frac{1}{\lambda_{\text{mag}}(T,\boldsymbol{S})} + \frac{1}{\lambda_{\text{def}}}. \tag{1}$$

λ stands for the electrons mean free path in the material and λ_i are, respectively, the electron-electron, electron-phonon, electron-magnon, and electron-defect mean free paths.

Of the scattering processes accounted for, only the electron-electron interaction is inelastic in nature; the others not resulting in significant energy loss, but rather momentum transfer. Electrons deviated from their initial trajectories are ejected out of the Schottky diode acceptance cone [35]. Unlike other kinds of elastic effects, magnons also affect the spin of charge carriers [36], $\boldsymbol{S}$, and incoming electrons can suffer a backward propagation and even a spin flip depending on their relative spin direction.

On the one hand, the probabilities of an electron-phonon [14] and electron-magnon [37] interaction increase much faster with temperature T than the probability of an electron-electron interaction, so that we will assume λ_e to be independent of T. On the other hand, the electron-electron interaction probability is strongly affected by energy. The frame of Fermi-liquid theory offers a description of single excited electrons interacting with the conduction electrons sea. This has been successfully used to determine the lifetime of excited electrons for a wide range of materials measured through two-photon photoemission spectroscopy [14,16]. Even though this theory neglects band structure effects, it has proven to be quite reliable for simple metals (Al) and noble metals (Cu,Ag,Au) [16]. Moreover, additional refinements taking into account the contribution of the d band to the electronic decay make this model suitable for the study of the electronic lifetime in noble or transition metals [38]. From Fermi-liquid theory and assuming a free-electron behavior, the dependence in energy of the inelastic mean free path can be described as

$$\lambda_e(E) = \lambda_0 \frac{\sqrt{E}}{(E-E_F)^2 + \varrho(E-E_F-\omega^{\uparrow})^2}, \tag{2}$$

where λ_0 stands for a characteristic value of the electron-electron interaction. E is the electron energy, E_F the Fermi level, ϱ a unitless coefficient related to the d-band density and, $\omega^{\uparrow}$ the energy shift between the upper part of the spin-up d band and the Fermi level. Equation (2) indicates that the more energetic the incoming electrons are (relative to the Fermi level), the shorter the inelastic mean free path. The contribution to the collector current of secondary electrons produced by inelastic scattering events has been neglected, such that the inelastic attenuation length becomes equal to the inelastic mean free path, and, that the contribution of the secondary electrons will be included separately.

In the last step, the electrons that overcome the Schottky-barrier height are collected in the semiconductor conduction band. In models developed for BEEM studies [26], a 5/2 power law of the collected current with kinetic energy is used. Because of the low height of the Schottky barrier and the low energy of the injected electrons, the impact ionization

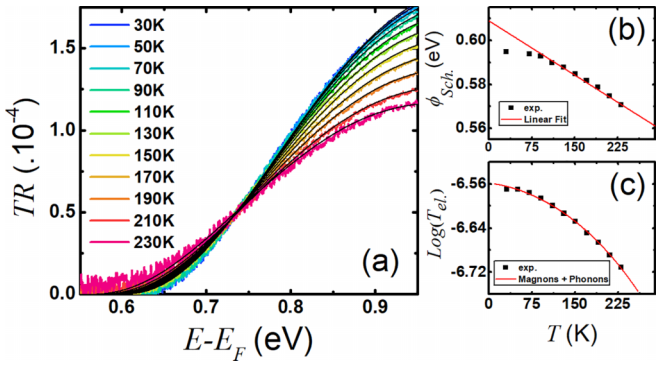

FIG. 2. (a) Experimental TR($E-E_F$) of the CoFeB(1) sample for several temperatures with associated fits. (b) Temperature dependence of Schottky-barrier height with linear fit over the [90, 230 K] region. (c) Temperature dependence of elastic transmission coefficient A. Theoretical model including magnons and phonons contribution is displayed.

and backscattering phenomena due to optical phonons in the semiconductor are neglected in our model [39].

From all the previous considerations we can write the transmission ratio TR as

$$\mathrm{TR}(T,\ V_{\mathrm{inj}}) = \frac{(|e|V_{\mathrm{inj}} - \phi_{\mathrm{Sch}}(T))^{5/2}}{I_{\mathrm{tun}}(V_{\mathrm{inj}})} T_{\mathrm{el}}(T) T_{\mathrm{inel}}(V_{\mathrm{inj}}), \quad (3)$$

where $\phi_{\mathrm{Sch}}(T)$ is the Schottky-barrier height. $T_{\mathrm{el}}(T) = T_0 \Gamma^n e^{-d_{\mathrm{base}}(1/\lambda_{\mathrm{ph}}+1/\lambda_{\mathrm{mag}})}$ stands for all the elastic processes with phonon and magnon attenuation lengths taken as effective values for the whole base stack, T_0 is a constant that takes into account the scattering induced by defects, Γ is a scattering coefficient due to the n interfaces present between each layer composing the base, d_i represents the thickness of the individual layer indexed i, and $d_{\mathrm{base}} = \sum d_i$ is the total thickness of the base. $T_{\mathrm{el}}(T)$ strongly depends on temperature but not on the electron energy. $T_{\mathrm{inel}}(V_{\mathrm{inj}}) = \prod e^{-d_i/\lambda_e^i}$ accounts for all the inelastic scattering processes which depend on the electron energy but not on the temperature.

IV. LOW ENERGIES REGIME (<1 eV)

In a first step, we considered the regime of hot electron transport for which produced secondary electrons are not contributing to $I_{\mathrm{col}}(V_{\mathrm{inj}})$ and studied $TR(V_{\mathrm{inj}})$ versus temperature and energy. Figure 2(a) shows measurements of TR vs V_{inj} made with the MTT including a 1 nm CoFeB layer in its base with temperatures ranging from 30 to 230 K. TR vs V_{inj} follows the same trend in the whole temperature range: it remains null as for all biases lower than the Schottky-barrier height ϕ_{Sch} (≈ 0.65 V) and starts to increase revealing the arrival of hot electrons in the silicon collector. As the temperature increases, for a fixed injection bias, the transfer ratio decreases.

The characteristic values for e^-/e^- can be extracted from the inelastic mean free path from literature for Cu and CoFeB: $\lambda_0^{\mathrm{Cu}} = 20\,\mathrm{nm}\,(\mathrm{eV})^{(3/2)}$ ignoring the d band (buried too deeply to affect the lifetime) [40,41] and $\lambda_e(E)$ is shown by BEEM to slightly differ from the Fermi-liquid theory for CoFeB [42]. Quinn's description of $\lambda_e(E)$ gives a value in good accordance with the experimentally measured inelastic mean free path, $\lambda_0^{\mathrm{CoFeB}} = 3.5\,\mathrm{nm}\,(\mathrm{eV})^{(3/2)}$. As far as CoNi is concerned, experimental values of $\lambda_0^{\mathrm{CoNi}}$ could not be found. Therefore, we studied the transport in devices with two different CoFeB thicknesses (1 and 4 nm), supposing that the inelastic mean free path in the sample with 1 nm CoFeB film will be dominated by that of the Co-Ni multilayer. By adjusting the energy position of the maximum of TR, which considers only the primary electrons, the experimental curves are reproduced with a value of $\lambda_0^{\mathrm{CoNi}} = 4.5\,\mathrm{nm}\,(\mathrm{eV})^{(3/2)}$. Finally, the remaining parameters needed to plot $\lambda_e(E)$ for all the materials included in the base are ϱ and $\omega^{\uparrow}$. ϱ is assumed to be similar for all transition metals, with $\varrho = 0.28$ (no unit) [38,42]. Values of $\omega^{\uparrow}$ are estimated from *ab initio* calculations being about 0.7 and 0.5 eV for CoFeB and CoNi, respectively [43]. $T_{\mathrm{inel}}(V_{\mathrm{inj}})$, that accounts for all the inelastic scattering processes in the base which depend on the electron energy but not on the temperature, can be plotted without any free parameter. As a result, the variation of $\phi_{\mathrm{Sch}}(T)$ and $T_{\mathrm{el}}(T)$ with temperature can be extracted from Fig. 2(a) and Eq. (3) since they are the only parameters that depend on temperature. A very good agreement with our measurements could be obtained (the fitted curves with the model are the solid gray lines) with the variations of ϕ_{Sch} and T_{el} as a function of T reported in Figs. 2(b) and 2(c), respectively. ϕ_{Sch} decreases slightly with increasing T (about 4%), following a linear behavior in the temperature range [90, 230 K]. The slope of -165 μV/K is similar to what has been reported in previous studies [44]. This confirms both the quality of our Schottky barrier and the reliability of our model in the low-energy range. $\mathrm{Log}(T_{\mathrm{el}})$ decreases with temperature and its variation can be well reproduced assuming a T^{-2} dependence. This dependence has been theoretically and experimentally found in the case of metallic thin films for temperatures up to 100 K [45–47], matching with the temperature range of our study.

V. HIGH ENERGIES REGIME (>1 eV)

In a second step, we increased the energy of the electrons up to 2.8 eV, and this without a breakdown of the tunnel barrier, showing its high quality. The corresponding TR vs V_{inj} measurements performed at 50 K on the 4-nm-thick CoFeB device are shown in Fig. 3(a) (black continuous curve). As expected, after a steep increase of TR for energies up to 1 eV, it reaches a maximum before decreasing. This decrease is related to the dominance of electron-electron scattering and is well reproduced by our model [dashed black curve in Fig. 3(a)] when secondary electrons produced by inelastic scattering are neglected. However, this decrease stops around 1.8 eV and TR starts to increase again: a new conduction channel has been opened for an energy between φ_{Sch} and $2\varphi_{\mathrm{Sch}}$. It is known that primary electrons after having interacted with the electrons of the Fermi sea, lose typically about half of their energy by exciting secondary electrons [Fig. 3(b)]. Therefore, injecting electrons with an energy above $2\varphi_{\mathrm{Sch}}$ will lead to an additional collection channel made of secondary electrons.

Besides the scattering of primary electrons with *sp*-band electrons around the Fermi level, the *d* band can as well

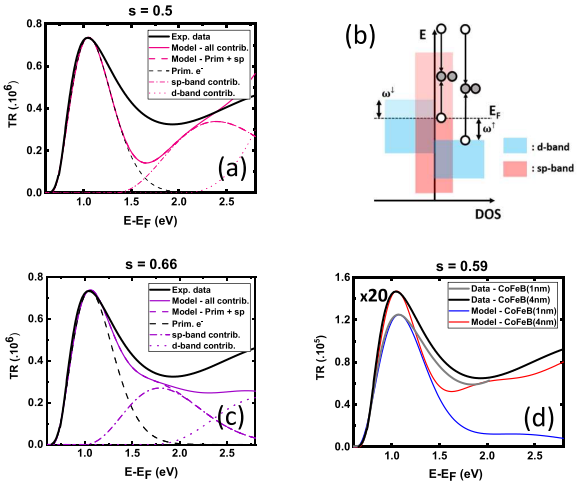

FIG. 3. (a), (c), and (d) TR versus energy. In all curves, the black line is the experimental TR($V_{\rm inj}$) values of the CoFeB(4) sample measured at 50 K and the gray line is the experimental TR($V_{\rm inj}$) values of the CoFeB(1) sample measured at 50 K. (b) Box bands diagram of a transition metal alloy with *sp* and *d* bands. Hot electrons above the Fermi level interact with electrons below E_F (white circles). This interaction generates two electrons at an intermediate energy (gray circles). Variation in the *s* parameter which rules the distribution of energy between ballistic hot electrons and that of the Fermi sea. It is equal to 0.5 (a), 0.66 (c), and 0.59 (d). In (a), (c), and (d), the black dashed line is the theoretical contribution of the primary electrons neglecting the secondary electrons produced by inelastic scattering. The colored dashed line is the theoretical contribution of the secondary *sp* electrons. The colored dotted line is the theoretical contribution of the total transmission including the secondary *sp* electrons. The colored light lines are the theoretical contribution of the secondary *d* electrons. The colored continuous line is the sum of all the theoretical contributions. The discrepancy between the model and experimental data in the case of CoFeB(1) is due to the generation of secondary electrons in the CoFeB layer being lower than that in the Cu and [Co/Ni] layers.

contribute to scattering. However, in this case the electron energy has to fulfill the following condition: $E > 2\phi_{\rm Sch} + \omega^{\uparrow}$ [see Fig. 3(b)]. Because of the high *d*-band density of states this contribution is expected to become comparable to that of the *sp* band. As a result, two additional channels of secondary electrons should open a channel related to *sp*-band interaction at $E \approx 2\phi_{\rm Sch}$ and a channel related to *d*-band interaction at around $E \approx 2\phi_{\rm Sch} + \omega^{\uparrow}$.

For the analysis of the secondary electron current, we have to take into account that primary electrons inelastically scattered in CoFeB, the number of which is proportional to $1 - e^{-t_{\rm CoFeB}/\lambda_e(V_{\rm inj})}$, can as well participate in the secondary electron current. However, not all of them are collected in the Si since the inelastic interaction can lead to a change of the wave vector such that the latter is no longer lying within the acceptance cone of the Schottky barrier. We have evaluated the amount of inelastically scattered electrons that are not collected [43] and take this into account by the introduction of two coefficients $C_{\rm sp}(V_{\rm inj})$ and $C_d(V_{\rm inj})$ for the *sp* and the *d* band, respectively. Both depend on $V_{\rm inj}$ and have values around 0.5.

The total transfer ratio related to the channels of secondary electrons can then be written as

$$\begin{aligned}
{\rm TR}_{\rm Sec.}^{\rm CoFeB}(V_{\rm inj}) = {} & \frac{\left(\frac{|e|V_{\rm inj}}{2} - \phi_{\rm Sch}\right)^{5/2}}{I_{\rm tun}(V_{\rm inj})} T_{\rm el} C_{\rm sp}(V_{\rm inj}) \\
& \times \left(1 - e^{-t_{\rm CoFeB}/\lambda_{\rm sp}^{\rm CoFeB}(V_{\rm inj})}\right) e^{-t_{\rm CoFeB}/\lambda_d^{\rm CoFeB}(V_{\rm inj})} \\
& \times \prod_j e^{-\left[d_j/\lambda_e^j(|e|V_{\rm inj}/2)\right]} \\
& + \frac{\left(\frac{|e|V_{\rm inj} - \omega\uparrow}{2} - \phi_{\rm Sch}\right)^{5/2}}{I_{\rm tun}(V_{\rm inj})} T_{\rm el} C_d(V_{\rm inj}) \\
& \times \left(1 - e^{-t_{\rm CoFeB}/\lambda_d^{\rm CoFeB}(V_{\rm inj})}\right) e^{-t_{\rm CoFeB}/\lambda_{\rm sp}^{\rm CoFeB}(V_{\rm inj})} \\
& \times \prod_j e^{-\left[d_j/\lambda_e^j\left(\frac{|e|V_{\rm inj} - \omega\uparrow}{2}\right)\right]}. \qquad (4)
\end{aligned}$$

The product $\prod_j e^{-d_j/\lambda_e^j}$ describes the inelastic scattering of the secondary electrons created in the CoFeB layer while they are crossing the remaining layers of the base (Cu and CoNi). The first term of Eq. (4) relates to secondary electrons arising from interactions with electrons from the *sp* band while the second term describes the secondary electrons coming from interactions with *d*-band electrons.

Without any free parameter, considering that primary electrons lose typically half of their energy by exciting secondary electrons, the theoretical contribution of secondary electrons has been added in Fig. 3(a) in the case of CoFeB(4 nm). Theoretically, increasing the hot primary electron energy leads to a reduction of λ_e [Eq. (2)] and thus to the reduction of the primary electron contribution to the collected current (black dashed line). When $|e|V_{\rm inj}$ exceeds $2\varphi_{\rm Sch}$, a contribution of secondary *sp* electrons (colored dashed line) appears that compensates the loss of primary electrons and the TR starts again to increase (colored dotted line−contribution of primary+secondary *sp* electrons). However, a further increase of $|e|V_{\rm inj}$ above 2.2 eV leads again to a reduction of TR. This last decrease is compensated by the appearance of the secondary *d* electrons channel (colored light lines). The sum of all the theoretical contributions (colored line) shows an increase as observed experimentally. As a result, both *sp*- and *d*-band contributions are needed to explain the experimental results.

While an equidistribution of energy between hot electrons and that of the Fermi sea has been considered by Quinn in his original paper [15], he predicted a repartition to be one-third/two-thirds. This would make the secondary *sp* and *d* electrons appear earlier in energy, limiting the deep in TR around 1.8 eV and the overshoot in TR at very high energies. Therefore, we simulate all the secondary contributions for secondary electrons having 2/3 of the primary ones. The results are reported in Fig. 3(c) in the case of CoFeB(4 nm). While the agreement is still not perfect, we limit the imperfections reported above. The best agreement with the experimental response has been obtained with a repartition 0.41/0.59 as shown in Fig. 3(d). In [48], Ritchie and Ashley clearly showed that the energy repartition depends on the electron/electron exchange: the repartition 0.5/0.5 (respectively, 0.34/0.66) is obtained with strong exchange (respec-

tively, without exchange). This could mean that part of the secondary electrons is created in the Cu layer of our spin valve. The experimental curve obtained on the device with 1 nm of CoFeB also points in this direction. Indeed, our model that considers only the creation of secondary electrons in CoFeB fails to reproduce the increase of TR after 1.8 eV. As a result, secondary electrons need to be also created in Cu.

In all cases, only transitions involving a majority-spin hot electron decaying into majority states have been considered. From the TMR of our device (55% at low voltage), one can evaluate the polarization to lie around 0.5 meaning that 75% of the incoming electrons will have a majority spin and 25% a minority one. As the minority spin electrons have a very short mean free path ($\sim$1 nm) in ferromagnetic layers, they relax quickly into the base and will give rise to an additional secondary electron channel. We introduced this channel in our model with a probability for incoming electrons to keep their spin while interacting to produce a secondary electron. In all cases, both *sp*- and *d*-band contributions are needed to explain our experimental results. We could also evoke the existence of spin flip processes between the two spin polarized channels, that could be elastic or inelastic. The elastic spin flip events, for minority or majority spin, occur through the emission or absorption of magnons. The last one becomes important in the presence of magnons. Considering the temperature used for our experiments, we neglect this process. The emission process is spontaneous. The change of wave vector is sufficient so that electrons are backward scattered. As a result, both elastic spin flip processes have no impact on the collected current. Vlutters *et al.* have drawn the same conclusion in their work [37]: Using a spin valve transistor, in an energy range close to the one studied here, they showed that the thermalization length is greater than 100 nm at low temperatures and decreases as the temperature increases. This leads to a decrease in TR. Finally, we measured the TR in our device as a function of temperature. For temperatures below 50 K, there is no influence of temperature on the TR. We thus show that elastic spin flip scattering has no impact on the secondary electron contribution. Let us now look at the spin flip process in inelastic scattering events. A process is rarely reported in literature, with most studies considering interacting electrons to remain in their respective spin channel (no spin flip). A theoretical work introduced a possible spin flip mechanism following an electron-electron interaction depending on both spin and energy (e.g., [49]). The calculations show that inelastic electron-electron scattering is not dominated by spin flip processes for Fe and Ni above 2 eV. Actually, there is no definitive conclusion on the spin-dependent transport of hot electrons in this energy range. Therefore, we do not go into those considerations here.

Finally, the assumption that only injected electrons with wave vectors $\boldsymbol{k}$ perpendicular to the interfaces have to be considered can be questioned. In a device similar to the one used in our study, the tunnel momentum distribution in an Al_2O_3 magnetic tunnel junction has been probed and exhibited a more isotropic current distribution [50]. While the current of primary electrons would not be altered, since it is limited by the acceptance cone of the Schottky barrier, the $\boldsymbol{k}$ vector distribution could give rise to additional secondary electrons collected in Si. Indeed, a $\boldsymbol{k}$ vector of a primary electron lying outside of the acceptance cone can nevertheless be reoriented towards the acceptance cone after scattering. As a result, the theoretical contribution of the secondary *sp* electrons (colored dashed line) and of the secondary *d* electrons channel (colored light lines) would be increased, thus leading to a better accordance between measurement and theory.

Thanks to the use of an MTT lab-on-chip device with a low height Si/Cu Schottky barrier, we were able to disentangle the different contributions to scattering in a metallic spin valve. The transport of hot electrons is reproduced in the light of electron-electron interactions, and generation of secondary electrons due to both *sp*- and *d*-band structures. The simple transport model can explain the experimental results as a direct consequence of secondary electron generation, both from *sp*-band (between 1.2 and 1.8 eV) and from *d*-band electrons (above 1.8 eV).

ACKNOWLEDGMENTS

We thank Yuan Lu for his help with the optimization of the Cu/Si Schottky barrier. This work has partially been supported by ANR SpinPress (ANR-09-BLAN-0076). Experiments were carried out on IJL Project TUBE-Davm equipment funded by FEDER (EU), French PIA project "Lorraine Université d'Excellence" (ANR-15-IDEX-04-LUE), Region Grand Est, Metropole Grand Nancy, and ICEEL. C.T. acknowledges funding from the project "MODESKY" ID PN-III-P4-ID-PCE-2020–0230, No. UEFISCDI: PCE 245/02.11.2021.

M.H. and D.L. conceived the project. V.D., M.H., and D.L. were in charge of the thin-film growth and optimization of magnetic properties. V.D. patterned the samples. V.D. and D.L. conducted the electronic transport under applied field experiment. C.T., V.D., W.W., D.L., and M.H. analyzed the data. D.L. and M.H. wrote the manuscript. All authors contributed to the discussion.

[1] H. Kroemer, Theory of the Gunn effect, Proc. IEEE **52**, 1736 (1964).

[2] M. Heiblum, M. I. Nathan, D. C. Thomas, and C. M. Knoedler, Direct observation of ballistic transport in GaAs, Phys. Rev. Lett. **55**, 2200 (1985).

[3] A. Othonos, Probing ultrafast carrier and phonon dynamics in semiconductors, J. Appl. Phys. **83**, 1789 (1998).

[4] S. M. Sze, *High-Speed Semiconductor Devices* (Wiley, New York, 1990).

[5] J. A. Kash and J. C. Tsang, Watching chips work: Picosecond hot electron light emission from integrated circuits, J. Cryst. Growth **210**, 318 (2000).

[6] P. V. Kamat, Capturing hot electrons, Nat. Chem. **2**, 809 (2010).

[7] *Laser Spectroscopy and Photochemistry on Metal Surfaces*, edited by H.-L. Dai and W. Ho (World Scientific, Singapore, 1995), p. 625.

[8] T. Kawahara, K. Ito, R. Takemura, and H. Ohno, Spin-transfer torque RAM technology: Review and prospect, Microelectron. Reliab. **52**, 613 (2012).

[9] S. Iihama, Y. Xu, M. Deb, G. Malinowski, M. Hehn, J. Gorchon, E. E. Fullerton, and S. Mangin, Single-shot multi-level all-optical magnetization switching mediated by spin transport, Adv. Mater. **30**, 1804004 (2018).

[10] Th. Fauster and W. Steinmann, in *Electromagnetic Waves: Recent Developments in Research*, edited by P. Halevi (Elsevier, Amsterdam, 1994).

[11] J. Bokor, Ultrafast dynamics at semiconductor and metal surfaces, Science **246**, 1130 (1989).

[12] C. A. Schmuttenmaer, M. Aeschlimann, H. E. Elsayed-Ali, R. J. D. Miller, D. A. Mantell, J. Cao, and Y. Gao, Time-resolved two-photon photoemission from Cu(100): Energy dependence of electron relaxation, Phys. Rev. B **50**, 8957(R) (1994).

[13] W. S. Fann, R. Storz, H. W. K. Tom, and J. Bokor, Electron thermalization in gold, Phys. Rev. B **46**, 13592 (1992).

[14] E. Knoesel, A. Hotzel, T. Hertel, M. Wolf, and G. Ertl, Dynamics of photoexcited electrons in metals studied with time-resolved two-photon photoemission, Surf. Sci. **368**, 76 (1996).

[15] J. J. Quinn, Range of excited electrons in metals, Phys. Rev **126**, 1453 (1962).

[16] M. Bauer, A. Marienfeld, and M. Aeschlimann, Hot electron lifetimes in metals probed by time-resolved two-photon photoemission, Prog. Surf. Sci. **90**, 319 (2015).

[17] M. Prietsch, Ballistic-electron emission microscopy (BEEM): Studies of metal/semiconductor interfaces with nanometer resolution, Phys. Rep. **253**, 163 (1995).

[18] V. Narayanamurti and M. Kozhevnikov, BEEM imaging and spectroscopy of buried structures in semiconductors, Phys. Rep. **349**, 447 (2001).

[19] R. Jansen, The spin-valve transistor: a review and outlook, J. Phys. D: Appl. Phys. **36**, R289 (2003).

[20] D. J. Monsma, J. C. Lodder, Th. J. A. Popma, and B. Dieny, Perpendicular hot electron spin-valve effect in a new magnetic field sensor: The spin-valve transistor, Phys. Rev. Lett. **74**, 5260 (1995).

[21] X. Jiang, R. Wang, S. van Dijken, R. Shelby, R. Macfarlane, G. S. Solomon, J. Harris, and S. S. P. Parkin, Optical detection of hot-electron spin injection into GaAs from a magnetic tunnel transistor source, Phys. Rev. Lett. **90**, 256603 (2003).

[22] S. van Dijken, X. Jiang, and S. S. P. Parkin, Nonmonotonic bias voltage dependence of the magnetocurrent in GaAs-based magnetic tunnel transistors, Phys. Rev. Lett. **90**, 197203 (2003).

[23] L. D. Bell, Evidence of momentum conservation at a nonepitaxial metal/semiconductor interface using ballistic electron emission microscopy, Phys. Rev. Lett. **77**, 3893 (1996).

[24] R. P. Lu, B. A. Morgan, K. L. Kavanagh, C. J. Powell, P. J. Chen, F. G. Serpa, and W. F. Egelhoff, Hot-electron attenuation lengths in ultrathin magnetic films, J. Appl. Phys. **87**, 5164 (2000).

[25] L. J. Schowalter and E. Y. Lee, Role of elastic scattering in ballistic-electron-emission microscopy of Au/Si(001) and Au/Si(111) interfaces, Phys. Rev. B **43**, 9308(R) (1991).

[26] M. Prietsch and R. Ludeke, Ballistic-electron-emission microscopy and spectroscopy of GaP(110)-metal interfaces, Phys. Rev. Lett. **66**, 2511 (1991).

[27] F. J. Garcia-Vidal, P. L. de Andres, and F. Flores, Elastic scattering and the lateral resolution of ballistic electron emission microscopy: Focusing effects on the Au/Si interface, Phys. Rev. Lett. **76**, 807 (1996).

[28] P. L. de Andres, F. J. Garcia-Vidal, K. Reuter, and F. Flores, Theory of ballistic electron emission microscopy, Prog. Surf. Sci. **66**, 3 (2001).

[29] A. Bauer, M. T. Cuberes, M. Prietsch, and G. Kaindl, Quantitative study of electron transport in ballistic-electron-emission microscopy, Phys. Rev. Lett. **71**, 149 (1993).

[30] C. Vautrin, D. Lacour, C. Tiusan, Y. Lu, F. Montaigne, M. Chshiev, W. Weber, and M. Hehn, Low-energy spin precession in the molecular field of a magnetic thin film, Ann. Phys. **533**, 2000470 (2021).

[31] C. Vautrin, D. Lacour, G. Sala, Y. Lu, F. Montaigne, and M. Hehn, Thickness and angular dependence of the magnetocurrent of hot electrons in a magnetic tunnel transistor with crossed anisotropies, Phys. Rev. B **96**, 174426 (2017).

[32] C. Vautrin, Y. Lu, S. Robert, G. Sala, O. Lenoble, S. Petit-Watelot, X. Devaux, F. Montaigne, D. Lacour, and M. Hehn, Magnetic tunnel transistor with a perpendicular Co/Ni multilayer sputtered on a Si/Cu(1 0 0) Schottky diode, J. Phys. D: Appl. Phys. **49**, 355003 (2016).

[33] R. Vlutters, O. M. J. van't Erve, R. Jansen, S. D. Kim, J. C. Lodder, A. Vedyayev, and B. Dieny, Modeling of spin-dependent hot-electron transport in the spin-valve transistor, Phys. Rev. B **65**, 024416 (2001).

[34] I. Appelbaum and V. Narayanamurti, Monte Carlo calculations for metal-semiconductor hot-electron injection via tunnel-junction emission, Phys. Rev. B **71**, 045320 (2005).

[35] A. F. J. Levi, J. R. Hayes, P. M. Platzman, and W. Wiegmann, Injected-hot-electron transport in GaAs, Phys. Rev. Lett. **55**, 2071 (1985).

[36] J. Hong and D. L. Mills, Spin dependence of the inelastic electron mean free path in Fe and Ni: Explicit calculations and implications, Phys. Rev. B **62**, 5589 (2000).

[37] R. Vlutters, O. M. J. van't Erve, S. D. Kim, R. Jansen, and J. C. Lodder, Interface, volume, and thermal attenuation of hot-electron spins in $Ni_{80}Fe_{20}$ and Co, Phys. Rev. Lett. **88**, 027202 (2001).

[38] E. Zarate, P. Apell, and P. M. Echenique, Calculation of low-energy-electron lifetimes, Phys. Rev. B **60**, 2326 (1999).

[39] R. Ludeke and A. Baue, Hot electron transport across metal-semiconductor interfaces probed by ballistic electron emission spectroscopy, Phys. Scr. **55**, 90 (1994).

[40] S. Ogawa, H. Nagano, and H. Petek, Hot-electron dynamics at Cu(100), Cu(110), and Cu(111) surfaces: Comparison of experiment with Fermi-liquid theory, Phys. Rev. B **55**, 10869 (1997).

[41] H. T. Nguyen-Truong, Low-energy electron inelastic mean free path in materials, Appl. Phys. Lett. **108**, 172901 (2016).

[42] S. van Dijken, X. Jiang, and S. S. P. Parkin, Spin-dependent hot electron transport in $Ni_{81}Fe_{19}$ and $Co_{84}Fe_{16}$ films on GaAs(001), Phys. Rev. B **66**, 094417 (2002).

[43] See Supplemental Material at http://link.aps.org/supplemental/10.1103/PhysRevB.108.214424 for ab initio calculations of

band structures and for the evaluation of the amount of inelastically scattered electrons that are not collected.

[44] M. O. Aboelfotoh, A. Cros, B. G. Svensson, and K. N. Tu, Schottky-barrier behavior of copper and copper silicide on *n*-type and *p*-type silicon, Phys. Rev. B **41**, 9819 (1990).

[45] J. F. DiTusa, K. Lin, M. Park, M. S. Isaacson, and J. M. Parpia, Role of phonon dimensionality on electron-phonon scattering rates, Phys. Rev. Lett. **68**, 1156 (1992).

[46] P. M. Echternach, M. E. Gershenson, and H. M. Bozler, Evidence of interference between electron-phonon and electron-impurity scattering on the conductivity of thin metal films, Phys. Rev. B **47**, 13659 (1993).

[47] J. Mathon and E. P. Wohlfarth, The temperature dependence of the spin wave energy in the itinerant electron model of ferromagnetism, Proc. R. Soc. London, Ser. A **302**, 409 (1968).

[48] R. H. Ritchie and J. C. Ashley, The interaction of hot electrons with a free electron gas, J. Phys. Chem. Solids **26**, 1689 (1965).

[49] V. P. Zhukov, E. V. Chulkov, and P. M. Echenique, Lifetimes of excited electrons in Fe and Ni: First-principles GW and the $T-$matrix theory, Phys. Rev. Lett. **93**, 096401 (2004).

[50] R. Jansen, T. Banerjee, B. G. Park, and J. C. Lodder, Probing momentum distributions in magnetic tunnel junctions via hot-electron decay, Appl. Phys. Lett. **90**, 192503 (2007).